JCTC Journal of Chemical Theory and Computation

Article

pubs.acs.org/JCTC

Reparameterized United Atom Model for Molecular Dynamics Simulations of Gel and Fluid Phosphatidylcholine Bilayers

Richard Tjörnhammar and Olle Edholm*

Theoretical Biological Physics, Department of Theoretical Physics, KTH Royal Institute of Technology, AlbaNova University Center, SE-106 91 Stockholm, Sweden

Supporting Information

ABSTRACT: A new united atom parametrization of diacyl lipids like dipalmitoylphosphatidylcholine (DPPC) and the dimyristoylphosphatidylcholine (DMPC) has been constructed based on *ab initio* calculations to obtain fractional charges and the dihedral potential of the hydrocarbon chains, while the Lennard-Jones parameters of the acyl chains were fitted to reproduce the properties of liquid hydrocarbons. The results have been validated against published experimental X-ray and neutron scattering data for fluid and gel phase DPPC. The derived charges of the lipid phosphatidylcholine (PC) headgroup are shown to yield dipole components in the range suggested by experiments. The aim has been to construct a new force field that retains and improves the good agreement for the fluid phase and at the same time produces a gel phase at low temperatures, with properties coherent with experimental findings. The gel phase of diacyl-PC lipids forms a regular triangular lattice in the hydrocarbon region. The global bilayer tilt obtains an azimuthal value of 31° and is aligned between lattice vectors in the bilayer plane. We also show that the model yields a correct heat of melting as well as decent heat capacities in the fluid and gel phase of DPPC.

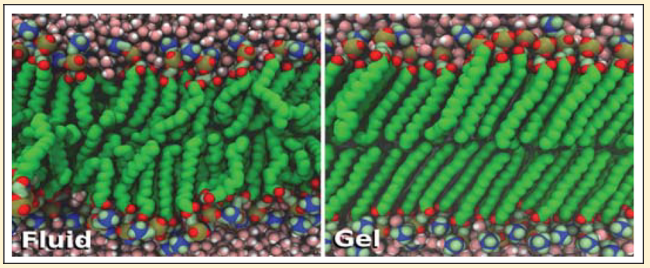

INTRODUCTION

Atomistic simulations of lipid bilayers have been performed for more than 25 years now.[1] With increasing computer speeds and improved force fields, results for the high-temperature phase (liquid crystalline, L_α or fluid phase) are getting more and more reliable. A few attempts have also been undertaken to simulate the low temperature gel phase.[2,3] To do this in true equilibrium requires, however, considerable computational efforts due to much slower dynamics. It has also become quite clear that many of the force fields that produce a good high temperature phase are not up to doing the gel well. The aim of the present communication is to show that a slight retuning of force-field parameters in the most common models results in a good description of both the fluid (L_α) and gel (L_β) phases (see Figure 1).

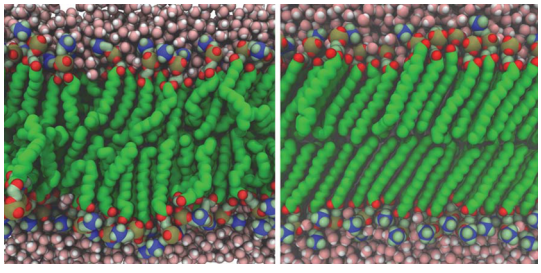

Figure 1. Snapshot from a simulation of a fluid (left) and gel (right) phase DPPC bilayer viewed along a lattice direction.

Lipid bilayers may be modeled at different levels of approximation. At one end there are coarse grained (CG) models,[4−6] with explicit or implicit water. They have the advantage that long time scales can be covered. They have relatively few parameters, and one can therefore fairly easily optimize these parameters to get the desired behavior of the model. The lack of detail and small number of parameters do, however, limit accuracy. At the other end, all atom (AA) models[7−9] can be investigated using more time-consuming but still doable simulations. We use a united atom (UA) representation of the hydrocarbon-groups, meaning that the nonpolar hydrogens are included into the carbons to form a neutral spherically symmetric united atom. Such models have been parametrized for lipid bilayer simulations by Berger et al.[10] and Chiu et al.[11,12] and many other authors. The philosophy taken here will be to determine fixed fractional charges and bonded parameters, including torsion potentials, from quantum mechanical simulations. In this work we show that a modified UA force field based on the Berger/Chiu[10,12] parametrizations can describe both the ordered gel phase and the liquid crystalline high temperature phase well. Previous UA representations of phospholipids do not produce the proper gel phase at low temperatures. This is seen in both the area per lipid, which for a pure DiPalmitoylPhosphatidylCholine (DPPC) bilayers ends up at 0.51−0.53 nm^2, and the general

Received: July 9, 2014
Published: October 30, 2014

   dx.doi.org/10.1021/ct500589z | *J. Chem. Theory Comput.* 2014, 10, 5706−5715

structure that is more reminiscent of the ripple (P_β) phase.[13] Experimental work indicates an area per lipid of 0.472 ± 0.05 nm[2][14,15] gel DPPC bilayers. The present reparameterization mends this problem.

METHODOLOGY

Since the dynamics is two magnitudes slower in the ordered phase than in the disordered one, we need to construct the initial gel structure. We utilized equilibrium gel phase structures from coarse grained (CG) MARTINI[5,16] simulations. Based on these structures UA structures were interpolated on top of the MARTINI beads. This is done by defining quaternion rotations with which the finer molecular structure can be aligned. Each MARTINI bead is as such assigned a set of UA particles with the restriction to the alignment process that the center of masses of both models should coalesce. By defining alignment vectors and grouping the beads together one can do this for any molecule. However, the interpolation will in general not conserve bond lengths that are defined for a specific force field. Thus, an interpolated structure must be properly energy minimized before molecular dynamics is performed. Since the chain tilt of the MARTINI gel is much less than the experimental tilt, the development of a correct tilt in the UA simulations constitutes an important validation for the force field. Alternatively, we tried to to put ordered lipids on a regular lattice and equilibrate through energy minimization followed by constant pressure molecular dynamics simulations. This resulted in similar final structure as those started from the MARTINI structures. Cooling of the fluid phase would also work, in principle, but was not utilized since it would require very long simulations (μseconds).

We choose to use a simple Lennard-Jones (LJ) model with united atoms for the nonpolar hydrocarbon groups. The interaction is described by the potential

$$V(r) = 4\epsilon\left(\left(\frac{\sigma}{r}\right)^{12} - \left(\frac{\sigma}{r}\right)^{6}\right) = \frac{C_{12}}{r^{12}} - \frac{C_6}{r^6} \quad (1)$$

This reduces the number of atoms and parameters of the model. Compared to a fully atomistic model[17] that includes the hydrogens of the CH_2-groups as separate atoms this simplification means that there is no electrostatics in the hydrocarbon region. It is clear from test simulations that the minute fractional charges of the hydrocarbons will give rise to a small electrostatic repulsion. The UA hydrocarbon groups have isotropic LJ-interactions, while the presence of explicit hydrogens in a fully atomistic model breaks the rotational symmetry. Still both models suffer from other approximations. The $1/r^{12}$ repulsion in the LJ-interactions is ad hoc and probably too weakly varying with distance. The fractional charges are fixed, while quantum mechanical (QM) calculations indicate that these depend upon the conformation.

The simulations were carried out using the GROMACS simulation package version 4.5.5[18] with a time step of 4 fs. Particle Mesh Ewald (PME) summation[19] with a real space cutoff of 1.0 nm was used for the electrostatics, while the LJ-interactions were calculated out to 1.0 nm every time step using a neighbor list to speed up the calculation. This was regenerated every 10 time steps. Between 1.0 and 2.0 nm the LJ-interactions were recalculated every time the neighbor list was generated. Finally, a spherically symmetric dispersion correction was calculated for the pressure and the energy and added outside 2.0 nm. The dispersion correction is of minor importance for the energies but has some effect on the pressure.

The systems were simulated at constant pressure and temperature. The temperature coupling algorithm used was the stochastic velocity rescaling thermostat[20] with a time constant of 100 fs and the appropriate reference temperatures. The pressure coupling utilized the semi-isotropic Berendsen barostat[21] with a time constant of 5 ps coupled to atmospheric pressure in all coordinate directions. To calculate the area compressibility from area fluctuations additional simulations were performed using the Parrinello−Rahman barostat.[22] All simulations where carried out for at least 100 ns, where the last 20 ns were used for sampling of averages.

The QM calculations were performed with the CPMD package [CPMD v.3.13, http://www.cpmd.org/ Copyright IBM Corp 1990−2008 Copyright MPI für Festkörperforschung Stuttgart 1997−2001.].[23] Entire molecules were simulated in separate runs with PBE and BLYP exchange correlation functionals employing Martin-Troullier (MT) pseudopotentials as well as Vanderbilt (VDB) ultrasoft pseudopotentials. Isolated molecular systems employing a plane wave energy cutoff of 85 Ry were used in all calculations for the MT potentials and 35 Ry for the VDB potentials. Separate calculations were performed to obtain partial charges and torsional potentials.

The DPPC system was constructed from 128 DPPC molecules and 4461 TIP4P/2005[24] water molecules. We did choose this four-site water model since it is the water model that best reproduces the properties of liquid water (and ice) across a wide range of temperatures.[25] The small size of the system is sufficient, although there is a finite size effect on the area per lipid in the fluid phase. This is negligible, when PME is used for the electrostatics.[26] The small system size means that system properties can be analyzed without having to take undulations into account.[27]

PARAMETERIZATION

The major changes to the force field are new partial charges based on QM calculations, a slightly different dihedral potential for the fatty acid chains and modified LJ-parameters for the tail chain UA-carbons. High level quantum chemistry calculations for *n*-alkanes are available in the literature,[28] and while a comparison between anisotropic hydrocarbons and isotropic united atom descriptions is not simple, we note that typical σ values have a range of 0.35−0.41 nm. A full discussion regarding why anisotropic united atom (AUA) interactions in *n*-alkanes (or AA) are needed to produce thermodynamic properties that scale correctly with pressure and temperature has been conducted by Toxvaerd.[29,30] We nevertheless refrain from using the AUA (or AA) description since correct density scaling with temperature can be achieved by simpler UA parametrization, see ref 31.

The torsional potential was determined by performing geometry optimization of single *n*-hexane and *n*-butane molecules. We allowed all degrees of freedom, except the torsional angle of the central bond, to relax during the optimization. The dihedral potential was constructed to include nonbonded 1−4 interactions. The final potential, designated "present", is shown in Figure 2. The QM derived torsion is similar to what is found in the CHARMM[8] force field but differs clearly from the OPLSA dihedral parameters used in the TraPPE force field.[31] The experimental potential comes from IR spectroscopic measurements conducted on *n*-butane.[32]

In the expanded dihedral energy

dx.doi.org/10.1021/ct500589z | J. Chem. Theory Comput. 2014, 10, 5706−5715

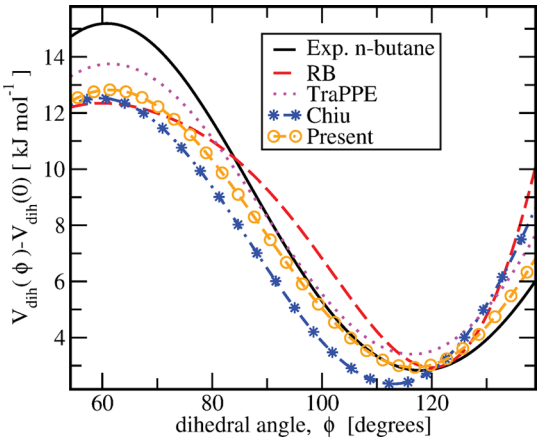

Figure 2. Different dihedral potentials for *n*-alkanes focused on the gauche minimum. The effective *n*-alkane QM dihedral potential employed in our classical simulations, compared to the classical Ryckaert-Bellemans one,[33] the TraPPE one,[31] the one of Chiu,[12] and an experimentally based one.[32]

$$V(\varphi) = \sum_{n=1} F_n[1 - \cos(n\varphi)] = \sum_{n=0} C_n[\cos(\varphi)]^n$$

with φ chosen according to the polymer convention, it suffices to include 3 Fourier coefficients, F_n. The trans state with $\varphi = 0$ will automatically have the energy zero. One needs $F_3 \approx 6-7$ kJ/mol to get appropriate barriers and in addition $F_1 \approx 2-4$ kJ/mol to get an energy of the gauche states around 3 kJ/mol. F_2 and the higher Fourier coefficients can be used to fine-tune the potential. In most of the potentials in Table 1, higher coefficients than F_3 are not needed. The exception is the classical Ryckaert-Bellemans potential[33] in which the higher coefficients are used to model the high cis barrier. The heights of the barriers are essential for the dynamics. For the equilibrium properties it is much more important to have the proper gauche energy. Since the gauche population is exponential in minus this energy over k_BT, results are sensitive to small alternations of this energy.The energies and positions of the gauche minima are presented in Table 1 for a few potentials. The steric hindrance will also affect the gauche minimum, making it less accessible in longer chains.

The Lennard-Jones parameters are most easily determined empirically from simulations of liquid *n*-alkanes. Experimental densities and heats of vaporization can be used to fix one C_6 and one C_{12} parameter. The problem is then that separate parameters for the CH_2-groups and the CH_3-groups are needed. One procedure to solve this is to use data for an entire series of hydrocarbons with different lengths.[12] It is, however, not so easy to get accurate data for the parameters in this way, since the CH_3-parameters have a small effect in the longer chains. It is interesting to note that different force fields[10,12,34] do come up with values for the quotient $C_6^{CH_3}/C_6^{CH_2}$ ranging from 1 up to 2.27 (average 1.45) using different arguments (or no arguments at all). One way to solve this is to use that the C_6-parameter in good agreement with high level *ab initio*[35] calculations can be expressed as

$$C_6 = \frac{3\hbar\omega}{4(4\pi\epsilon_0)^2}(n_{CH}\alpha_{CH} + n_{CC}\alpha_{CC})^2 \quad (2)$$

where n_{CH} is the number of carbon−hydrogen bonds, $\alpha_{CH} = 7.008 \times 10^{-41}$ As m^2/V is the polarizability of these bonds, n_{CC} is the number of carbon−carbon bonds, and $\alpha_{CC} = 6.527 \times 10^{-41}$ As m^2/V is the polarizability of the carbon/carbon bonds and the angular average frequency $\omega = 2.369 \times 10^{16}$ s^{-1} of the dipole fluctuations. ϵ_0 is the electric permittivity of vacuum. Applying eq 2 to the UA hydrocarbons readily yields the attractive Lennard-Jones parameters of the CH- and CH_3-groups in terms of the CH_2-one as

$$C_6^{CH_3} = 1.3978C_6^{CH_2} \text{ and } C_6^{CH} = 0.6687C_6^{CH_2} \quad (3)$$

Equation 2 gives also an absolute value for the C_6-parameter of the CH_2-groups, 3.866×10^{-3} kJ mol^{-1} nm^6. The repulsive LJ parameter is still unknown but may be determined by requiring that the density agrees with experiment for a given C_6-parameter. This gives a linear relation between the C_{12} and C_6 parameters of the CH_2-groups

$$C_{12}^{CH_2} = -1.1561\cdot10^{-5} + 6.1342\cdot10^{-3}C_6^{CH_2} \quad (4)$$

where the $C_{12}^{CH_2}$ has the unit kJ mol^{-1} nm^{12}. See Figure 3. This yields densities close to the experimental ones for all *n*-alkanes as seen in Figure 4. Next we need to fix the attractive C_6 parameter. We note then that a value that is about twice the value obtained from eq 2 is needed to get a correct heat of vaporization (see e.g. ref 12). We did finally choose to determine $C_6^{CH_3}$ to reproduce the experimental heat of vaporization of ethane at 184 K to avoid dependence on the dihedral potential. The $C_6^{CH_2}$ parameter was then determined from eq 3 and the repulsive LJ parameter from eq 4. The final test of the parameters obtained in this way is that they give densities and heats of vaporization at 293 K for the entire series of hydrocarbons (up to pentadecane) in agreement with experiment (see Figure 4).

In the most direct interpretation of the LJ-potential a smaller σ should yield a higher density. In analogy, going from larger to smaller ϵ should yield a decreasing heat of vaporization. It is however clear that small and large σ can both yield the same density. It is thus clear that a small σ yields a low melting temperature and low density in the fluid. A high ϵ yield dense fluids and high melting temperature. For the partial charges, we employ the same numbering of the atoms as in Berger et al.[10] and Chiu et al.[11] (Figure 5). We denote these force fields with

Table 1. Gauche Energies, E_g [kJ/mol], Barrier Energies, E_b [kJ/mol], Gauche Minima, φ_g [degrees], and Fourier Coefficients, F_n [kJ/mol], of Some of the Dihedrals Potentials for *n*-Alkanes

dihedral	E_g	E_b	φ_g	F_1	F_2	F_3	F_4	F_5
Exp.	2.82	15.2	118	1.41	0.22	6.83	0.20	0.07
RB	2.94	12.3	120	9.81	−6.56	10.61	−3.26	1.97
TraPPE	3.41	13.7	116	2.95	−0.57	6.58	0.	0.
Chiu	2.35	12.5	113	4.34	−2.43	7.01	0.	0.
QM	2.94	13.2	116	2.96	−0.90	6.55	0.	0.
present	2.94	12.8	116	2.57	−0.55	6.175	0	0

dx.doi.org/10.1021/ct500589z | J. Chem. Theory Comput. 2014, 10, 5706−5715

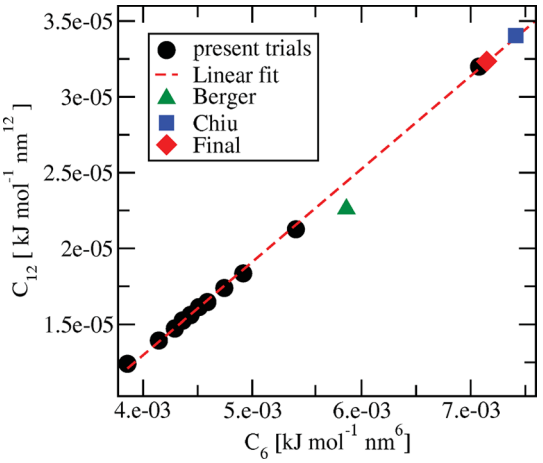

Figure 3. Repulsive LJ parameter versus the attractive one for hydrocarbon liquids with the correct density (at 298 K). The lowest value for the attraction is obtained from density functional theory while the highest one reproduces experimental enthalpies. The linear fit refers to eq 4.

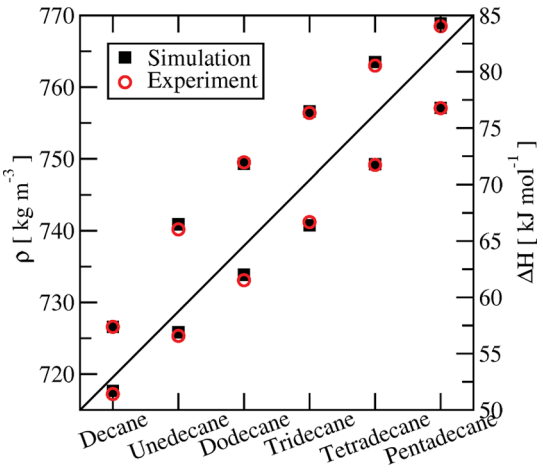

Figure 4. Comparison of experimental[36] and simulated densities of the higher alkanes. The temperatures are 298 K for decane and 293 K for the higher alkanes. The density for tetradecane was taken from the 58th edition of the CRC Handbook since there is an obvious misprint in the 88th and 92nd editions. A comparison of experimental and simulated enthalpies at 298 K is also included.

the Berger and Chiu, respectively. The bonded and nonbonded parameters not explicitly given here were taken as in the Berger force field.

In order to determine the partial charges of the atoms in the DPPC molecule an electrostatic potential fitting method was employed for 72 different all-atom DPPC configurations. These were taken from the last frame of an equilibrated bilayer of Klauda et al.[8] The entire molecule was simulated, and the resulting atomic charges were summed up into the UA atoms. This method yields a mean partial charge and a standard deviation of the partial charge coming from the differences between conformations and between different methods to determine the charges. The resulting charges are shown in Table 2. These charges are not far from those computed for a recent all atom model.[9] Performing gas phase QM-calculations on glycerol using B3LYP/6-31G* readily yields an evenly distributed backbone carbon partial charge of 0.24 per carbon. We note that our calculated average glycerol carbon charge falls within this value, but that it is reorganized across the backbone. This shows that there is a polarizing effect from the headgroup and carbonyl dipoles on the glycerol backbone. Our final values were chosen at the high end of the distribution. The carbonyl dipole strength was taken as a variable, but it is clear that other recent phospholipid descriptions[8,9,34] are converging close to our values. Poger et al.[34] duly notes that a low fractional charge of the carbonyl dipoles will drive the bilayer into an ordered low area phase. The partial charge of the choline nitrogen atom can be assessed, using the electronegativity of nitrogen and carbon to be $q_N \approx +0.65$. This is high but indicative of the sign.

Calculation of the headgroup dipole for the QM conformations yields $\langle\mu\rangle \pm \sigma_\mu = 19.3 \pm 5.5$ D. For the finally chosen charge distribution, a slightly higher value, 21.4 D, is obtained, which happens to agree with a recently suggested value based on *ab initio* calculations[37] and falls in the middle of the experimentally suggested interval, 18 to 25 D.[38,39]

VALIDATION

Some technical details of the simulations were first validated. This included the time step which was set to 4 fs based on experiences from fluid phase simulations in which water limits the size of the time step. Simulations with the smaller time step of 2 fs did not indicate any difference that called for a smaller time step than the original one. The twin-range cutoff scheme for the Lennard-Jones interactions was also tested by using a 2 nm cutoff every time step, and this did not produce any different results. We looked for finite size effects by performing simulations of larger systems containing 144, 576, and 1296 DPPC molecules. In agreement with earlier PME-simulations of fluid lipid bilayers,[26] we only observed a tiny finite size effect.

The initial structures were generated in different ways to test for a possible effect of the initial state. We either started from MARTINI-gel structures or by placing ordered phospholipids on a grid. In both cases, we started with the wrong collective tilt and the wrong area per lipid. Still, the system evolved during the simulations toward the same collective tilt and area per lipid, both in agreement with experiment. We also tried to generate the gel by annealing the fluid phase structures. In coarse grained MARTINI simulations the annealing could be

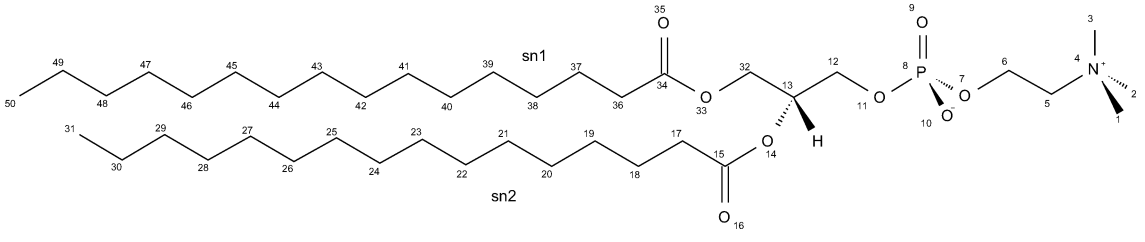

Figure 5. Numbering of the united atoms in DPPC.

dx.doi.org/10.1021/ct500589z | J. Chem. Theory Comput. 2014, 10, 5706−5715

Table 2. Fractional Charges of the 50 UA in DPPC[a]

n	atom	QM	PRES	CHIU	CHRM	JÄMB
1	C_γ	0.084 ± 0.069	0.10	0.40	0.40	0.19
2	C_γ	0.083 ± 0.057	0.10	0.40	0.40	0.19
3	C_γ	0.087 ± 0.044	0.10	0.40	0.40	0.19
4	N	0.473 ± 0.118	0.50	−0.50	−0.60	0.20
5	C_β	−0.007 ± 0.066	0.00	0.30	0.40	−0.02
6	C_α	0.300 ± 0.060	0.30	0.40	0.10	0.23
7	O	−0.514 ± 0.054	−0.50	−0.80	−0.57	−0.49
8	P	1.400 ± 0.114	1.35	1.70	1.50	1.58
9	O	−0.805 ± 0.040	−0.80	−0.80	−0.78	−0.86
10	O	−0.809 ± 0.034	−0.80	−0.80	−0.78	−0.86
11	O	−0.467 ± 0.065	−0.50	−0.70	−0.57	−0.49
12	C_g	0.141 ± 0.081	0.15	0.40	0.10	0.03
13	C_g	0.390 ± 0.111	0.50	0.30	0.26	0.52
14	O	−0.434 ± 0.072	−0.40	−0.70	−0.49	−0.47
15	C_c	0.765 ± 0.086	0.75	0.70	0.90	0.79
16	O_c	−0.586 ± 0.044	−0.75	−0.70	−0.63	−0.65
17	CH_2	−0.123 ± 0.068	0.00	0.00	−0.04	0.00
18	CH_2	0.073 ± 0.079	0.00	0.00	0.00	0.00
19	CH_2	0.017 ± 0.077	0.00	0.00	0.00	0.00
20	CH_2	−0.018 ± 0.073	0.00	0.00	0.00	0.00
...	CH_2	...	0.00	0.00	0.00	0.00
30	CH_2	0.079 ± 0.130	0.00	0.00	0.00	0.033
31	CH_3	−0.079 ± 0.075	0.00	0.00	0.00	−0.033
32	C_g	0.197 ± 0.089	0.30	0.50	0.26	0.25
33	O_g	−0.412 ± 0.075	−0.40	−0.70	−0.49	−0.47
34	C_c	0.775 ± 0.069	0.75	0.80	0.90	0.79
35	O_c	−0.584 ± 0.036	−0.75	−0.60	−0.63	−0.65
36	CH_2	−0.121 ± 0.061	0.00	0.00	−0.04	0.00
37	CH_2	0.078 ± 0.082	0.00	0.00	0.00	0.00
38	CH_2	0.010 ± 0.080	0.00	0.00	0.00	0.00
39	CH_2	−0.002 ± 0.080	0.00	0.00	0.00	0.00
...	CH_2	...	0.00	0.00	0.00	0.00
49	CH_2	0.095 ± 0.089	0.00	0.00	0.00	0.033
50	CH_3	−0.092 ± 0.100	0.00	0.00	0.00	−0.033

[a]QM denotes QM derived charges and are given with standard deviations. PRES denotes the present final choice of charges (PRES), CHIU the charges of Chiu et al.[11] (also used in refs 10 and 12). AA charges (summed into UA) from ref 8. (CHRM) and Jämbäck and Lyubartsev (JÄMB)[9] are also included.

done in about 50 μs. The dynamics is, however, about 1 order of magnitude slower in UA simulations[51] and would thus require 0.5 ms of simulation. This is unfeasible for the UA systems with present computer speeds. Simulating 144 lipids at full hydration along the freezing and melting transition in accordance with a previous UA study[50] at the annealing rate of 0.1 K ns^{-1} resulted in a transition in 500 ns. The system showed considerable hysteresis, and the final structures exhibited frozen-in disorder defects. This indicates that much slower annealing rates are required. Therefore, we decided to give up these efforts.

Some structural properties are tabulated in Table 3. From the simulated trajectories an average dipole moment of the phospholipid headgroup of 21.4 D was calculated, with the normal component equal to 8.1 D. The tilt of the dipole is known from NMR experiments.[39] From this a normal component in the range 6.5−9.5 D can be calculated. We note that both the Berger and Chiu force fields yield larger dipole moments, 24 and 26 D, respectively.

The area compressibility modulus can be determined from the area fluctuations, σ_A, as

Table 3. Some Properties of Fluid and Gel DPPC Bilayers[a]

property	exp.	P	B	C
T [K]	323	323	323	323
v_L [Å^3]	1230	1210	1256	1211
a_L [Å^2]	63.5	63.2	62.3	63.4
K_A [mN m^{-1}]	250	310	347	504
$\langle\mu\rangle$ [D]	21.5	21.4	23.9	26.5
$\langle\mu_\perp\rangle$ [D]	8	8.1	11.5	10.4
T [K]	293	293	283	283
v_L [Å^3]	1144	1130	1147	1130
a_L [Å^2]	47.3	47.7	51.2	53.1
K_A [mN m^{-1}]	1500	1450	1369	696

[a]B denotes the Berger, C the Chiu, and P the present force field.

$$K_A \equiv A\left(\frac{\partial\gamma}{\partial A}\right)_{T,V} = \frac{Ak_BT}{\sigma_A^2} \quad (5)$$

which yield 310 mN m^{-1} for the fluid phase and 1450 mN m^{-1} for the gel, close to the experimental figures. For both the Berger and Chiu force field the area per lipid is about 14% too large at gel temperatures, as a result of these stabilizing an

dx.doi.org/10.1021/ct500589z | J. Chem. Theory Comput. 2014, 10, 5706−5715

intermediate structure. The area is substantially improved with the new parametrization which results in a value of 0.475 nm^2 at 283 K and 0.477 nm^2 at 293 K, in agreement with experiment. The present parametrization does not change the properties of the fluid phase much and gives an area per lipid of 0.632 nm^2 at 323 K.

In experiments, the electron densities are not directly accessible but must be retrieved from the inverse Fourier transform of the structure factors. From the simulation, the structure factors can be calculated from the simulated electron densities, $\rho(z)$ as

$$F(q_z) = \int_{-D/2}^{D/2} (\rho(z) - \rho_w) \cos(zq_z)dz \quad (6)$$

Here ρ_w is the constant electron density of bulk water. The calculated structure factors for the gel and fluid phases are shown in Figure 6. We also estimate the difference between the

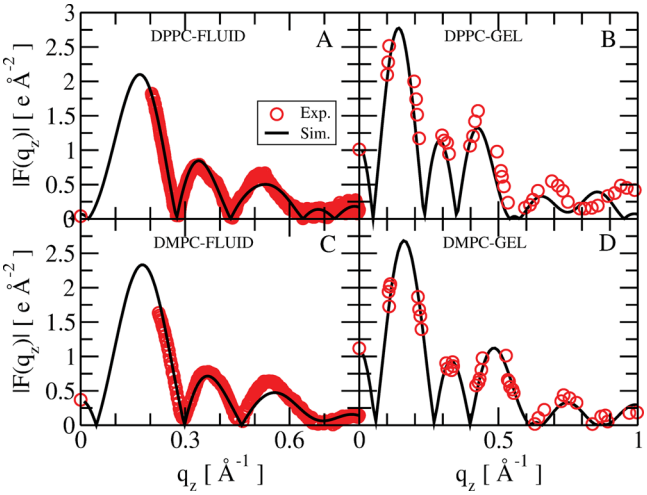

Figure 6. A comparison of the X-ray structure factors calculated from different simulations and experiments. *A:* (DPPC) Experimental fluid phase[40] together with the simulated data set. *B:* (DPPC) Gel phase experimental data[41] together with a single simulation integrated over different z-ranges. *C*: Structure factors of DMPC fluid phase and *D*: (DMPC) gel phase. Experimental data were taken from ref 42.

simulated data and the experimental data using a χ^2-test as suggested by Kucerka et al.[43] In the fluid phase we obtain χ^2-values of 1.23, 0.85, and 0.73 for the Berger, Chiu, and present force field, respectively. In the gel we do not come further down than to 3.8. It should be noted that the χ^2-values depend upon the error estimate for the experimental data.

We may, in a similar fashion, also calculate the neutron scattering length density and integrate it in order to obtain the neutron structure factors. We have taken scattering length data from NIST [http://www.ncnr.nist.gov/resources/n-lengths/] and calculated the average scattering length for each UA particle. These can easily be compared with experiments carried out at different D_2O concentrations by Kucerka et al.[44] (Figure 7). The χ^2-values for our gel phase neutron scattering profiles are 2.7−7.5 depending on deuterium level. The χ^2-values of the data shown in the figures are shown in Table 4. The absolute value of the structure factors at $q = 0$ are also shown in the figures. They were obtained as

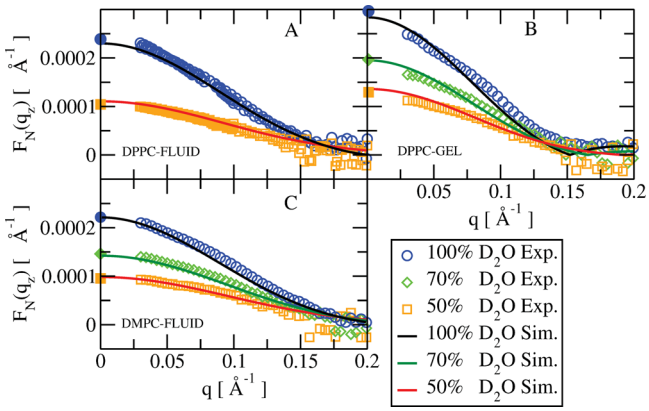

Figure 7. Calculated and experimental[44] neutron structure factors. The filled symbols at $q = 0$ were calculated from eq 7. *A*: DPPC fluid phase. *B*: DPPC gel phase. *C*: DMPC fluid phase.

Table 4. χ^2-Values for the Comparison of Experimental and Calculated X-ray and Neutron Scattering (at D_2O Concentrations from 50−100%) Profiles

lipid	phase	X-ray	neutron,50	neutron,70	neutron,100
DPPC	fluid	0.7	2.6		3.7
DMPC	fluid	0.8	2.5	2.8	4.5
DPPC	gel	3.8	2.7	3.6	7.5
DMPC	gel	4.0			

$$F_0 = \frac{2v_L}{a_L}(\rho_L - \rho_w) = \frac{2v_L}{a_L}(\rho_L - (f_D\rho_w^D + (1 - f_D)\rho_w^H)) \quad (7)$$

in accordance with ref 41 from the difference in electron density or neutron scattering length density between lipid and water, $\rho_L - \rho_w$, and the experimental area and volume per lipid. The total neutron scattering length densities are 2.2875×10^{-7} $Å^{-2}$, 2.8585×10^{-7} $Å^{-2}$, 6.3917×10^{-6} $Å^{-2}$, and -5.5992×10^{-7} $Å^{-2}$ for DPPC, DMPC, deuterium, and water, respectively. f_D denotes the fraction of deuterium in water. The average relative deviation between the structure factors obtained from simulations and those from X-ray scattering and neutron scattering are similar (0.25−0.30). Error estimates assigned to experimental data have a large influence on the χ^2-values, and the model discrepancy lies outside of the experimental accuracy. The X-ray and neutron scattering data covers to a large extent different wavenumber intervals, but even if they were to overlap a comparison is difficult since different atoms contribute differently to the two types of scattering. In order to check that the agreement with experiment is not a lucky coincidence, we have also chosen to simulate DMPC. We note that the fluid phase area-per-lipid as well as structure factors are all in good agreement with experiment. In the fluid phase we find the area per lipid 61.0 $Å^2$ and lipid volume of 1086 $Å^3$ for DMPC. Both figures are in decent agreement with the experimental values a_L = 60.6 $Å^2$ and v_L = 1100 $Å^3$.[45] For the DMPC gel we obtain, however, an area per lipid that is 1.9 $Å^2$ too large when simulated at 283 K. Simulating DMPC at 263 K reduces this error to 0.7 $Å^2$.

It is noteworthy that the Berger lipid UA parametrization yields both gel and fluid phase with correct volume densities and head−head distance (D_{HH}) despite that the area per lipid is too large in the gel phase. The structure as a whole is not in agreement with experimental findings for the L_β-phase but

dx.doi.org/10.1021/ct500589z | J. Chem. Theory Comput. 2014, 10, 5706−5715

more reminiscent of the P_β-phase. The new parametrization yields an area per lipid that is similar to the experimental one. The electron density of the new model is also much more structured than that of the older ones, see Figure 8B. Note that

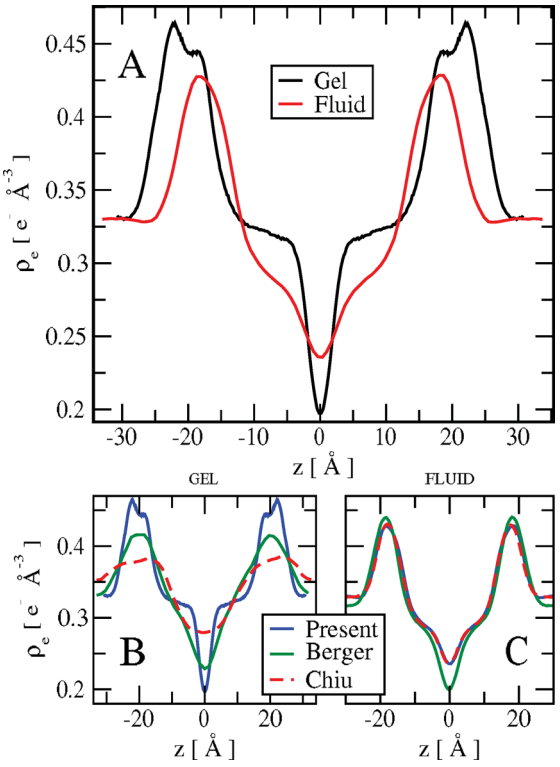

Figure 8. Calculated electron densities from the simulations. *A*: Comparison of the fluid and the gel for the present force field. *B*: Comparison of the Berger, Chiu, and present force field for the gel. *C*: Comparison of the Berger, Chiu, and present force field for the fluid.

in Figure 1 all lipids have an azimuthal tilt close to 30° but that there is a slight difference of polar ordering in the leaflets. The chains are colinear in both monolayers, which also is in agreement with experimental findings.[46] We also find weak correlations between the lattice vectors, in the hydrocarbon chain region, and other local lipid properties. The tilt direction can be seen to globally order between one of the lattice vectors as well as the carbonyl dipoles of the chains that order along a lattice vector. The tilt is perpendicular toward nearest neighbors which would indicate that we are in the $L_{\beta I}$ phase.[46] The fluid phase Berger lipids have a far too large volume of the CH_3-groups compared to the CH_2-ones.[47] This is reflected in the dip of the electron density in the center of the bilayer (where the CH_3-groups dominate).[48] As seen from Figure 8 the new force field produces an electron density that has a dip that is much more similar to that of Chiu et al.[12] This is also reflected in a similarly improved ratio of the CH_3 to CH_2 volumes. The main reason for the poor electron densities of the earlier UA models at low temperatures is that highly interdigitated states form. These will be stable for long times and are not physically unreasonable in a gel phase, but experiments show that DPPC membranes at 283 K do not contain a large amount of such states. We know that the UA gel phase can form with quite a spread in tilt angles of the lipid and with differently sized interdigitated regimes.[49,50]

RESULTS

The tilt of the gel phase chains is 31.0° ± 1° when calculated from the first to last hydrocarbon unit and averaged over the two chains (see Figure 9A). The experimental value is reported

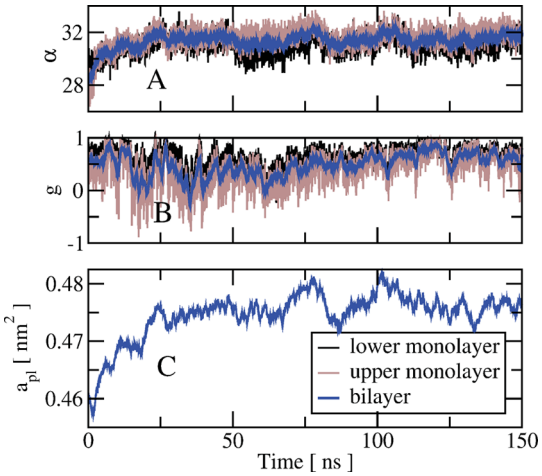

Figure 9. Lipid chain tilt (α) (A), chain rotation order parameter (g) (B), and projected area per lipid (C) versus time in the gel phase. The blue curves in A and B include some running averaging and averaging over the two monolayers.

to be 32° ± 0.5°.[14] The essentially straight, all-trans chains may also rotate around their long axis. The rotation can be characterized by an angle γ, that may be defined as the angle between the flat plane of the all trans chain and the plane formed by the tilt direction and the membrane normal. The angle γ takes then on values in the interval 0 to 90°, with 0 corresponding to a knife-like tilt into the membrane (with the plane of the chain parallel to the tilt plane) and 90 corresponding to a flat orientation with the chain plane being perpendicular to the tilt plane. An experimentally accessible order parameter can be defined[52] as $g = 2\langle\cos^2\gamma\rangle - 1$. A knife-like orientation would give $g = 1$, a flat one $g = -1$, while values close to 0 indicates rotational disorder. Experiments[52] indicate a small negative value (−0.3) of the order parameter, while the present simulations (Figure 9B) give +0.4. Thus, the simulations indicate a slight preference for an orientation with the knife edge of the lipid chains cutting into the membrane, while experiments indicate a slight preference for a more flat orientation. If there were no disorder, the experimental value would correspond to an angle of 54°, while the simulations would correspond to 33°. The present simulations indicate, however, a broad distribution width ±33° in this angle. The two-dimensional radial distribution function, calculated for the hydrocarbon chain region, shows that the chains in the gel phase form a well ordered lattice but that there is significant density between the lattice positions. Lattice defects and thermal spread contribute to this density. This is visible in Figure 10 as stripes in the 2D radial distribution function. The tilt vector is aligned perpendicular with one of the 2D lattice vectors, and the two monolayer leaflets have lattice vectors as well as tilt aligned. We also calculated the number of nearest neighbors by performing Voronoi tessellation and obtained 6 ± 0.5 for the gel and 6 ± 1.1 for the fluid phase. This means that there is an appreciable number of lattice defects also in the gel. From the area per lipid (0.477

dx.doi.org/10.1021/ct500589z | J. Chem. Theory Comput. 2014, 10, 5706−5715

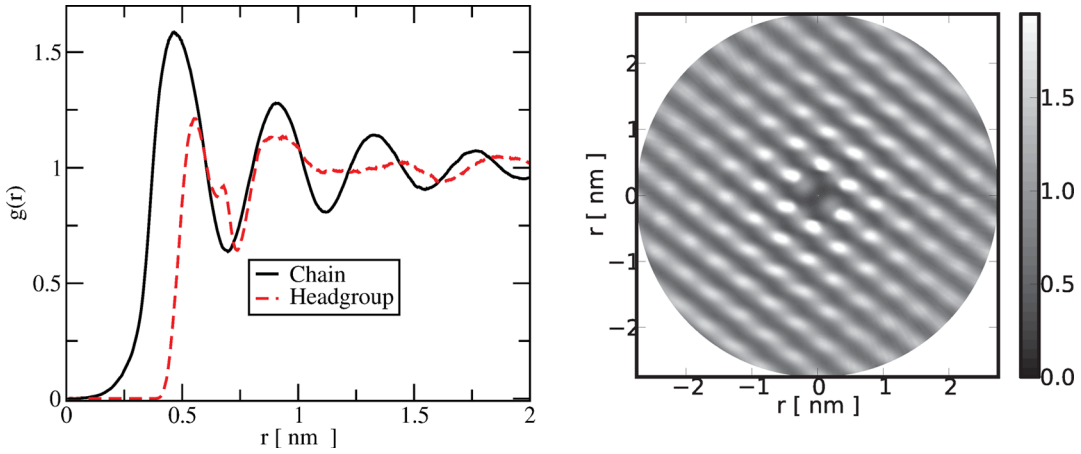

Figure 10. Radial distribution function for the headgroup region and the hydrocarbon tail in the gel phase. Density distribution in 2D of the carbon tail region.

nm^2), the tilt (31°) bond length and bond angle, the volume per CH_2 group can be calculated as 0.0258 nm^3.

The distribution of the angle between the in-plane lattice vectors connecting nearest-neighbor chains (not lipids) and the collective tilt direction (projected into the plane) is shown in Figure 11. It is clearly seen that the tilt is directed in between

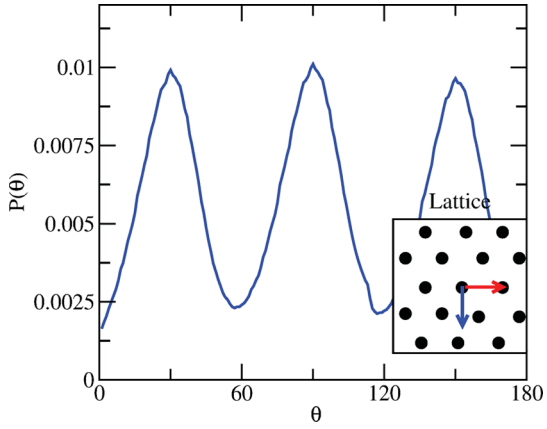

Figure 11. Angular distribution of the global chain tilt with respect to the lattice directions in the bilayer plane. The red arrow in the inset signifies a lattice vector chosen randomly in one of the six directions, while the blue arrow represents the global tilt direction.

two of the lattice vectors and thus form the angles ±30, ±9.0, and ±150° with the different lattice vectors. The peak width is about ±15°. For a large system one would expect the tilt direction to become decorrelated at long distances and even that the system has domains with different tilt directions. The present systems are too small to make a direct observation of this possible.

We note further, that the P−N dipole orientation in the membrane plane does not correlate with the chain tilt or the lattice directions. The relative orientation of nearest neighbor head-groups dipoles falls in directions that minimize the electrostatic interactions energy. This introduces short-range correlations which, however, fall off rapidly with distance since the weak dipole−dipole interactions are strongly screened by the water in a similar way as observed earlier in the fluid.[26]

The order parameters for the CH_2 particles, corresponding to the experimental S_{CD} order parameters, were calculated as an average over the two virtual C−H-bonds (uniquely defined from the backbone structure).

$$S_{CH} = S_{CD} = \frac{3 < \cos^2 \theta_{CH} > -1}{2} \tag{8}$$

The order parameter in the fluid phase varies from −0.2 in the top part of the chains to below −0.1 close to the chain ends. As seen from Figure 12A there is good agreement with experimental NMR order parameters. We have not been able to find NMR-order parameters resolved along the chain for the gel phase, but data from ref 53 for the first and second moments of the deuterium NMR spectra (and later similar measurements) indicate an average order parameter of around (−)0.43. The present gel phase data in Figure 12A agree with this. The ordering of the chains may also be characterized by the fraction of gauche and trans bonds. In the fluid phase these numbers are around 25% (75%) along most of the chain. See Figure 12B. In the gel phase the fraction of gauche bonds is about 4% in the most ordered central part of the chains and slightly higher in the beginning and especially at the end of the chains. This means that there will be on average about 1.5 gauche bonds per lipid (0.75 per chain). This is consistent with experimental results from Rahman scattering.[54]

The phase transition enthalpy can be calculated from the difference in total energy between the two phases (pressure−volume work is negligible). This will, however, be an overestimate since the two phases are simulated at different temperatures. Hysteresis and finite size broadening makes it difficult to exactly locate the melting temperature and do the simulation of both phases at this temperature. Instead, we estimate the heat capacity of the two phases

$$C_p \equiv \left(\frac{\partial H}{\partial T}\right)_p \tag{9}$$

from the enthalpy at different tempratures. By binning in temperature and extrapolating from above and below to the assumed melting temperature 313 K (see Figure 13), the phase transition enthalpy could be estimated. The classical heat capacities for the gel and fluid phase respectively were also obtained by subtracting the bulk water contribution from the enthalpy or total energy and calculating the derivative per lipid. Since we employ a stochastic thermostat, we have used the uncorrelated fluctuation data in order to obtain the red raw data

dx.doi.org/10.1021/ct500589z | J. Chem. Theory Comput. 2014, 10, 5706−5715

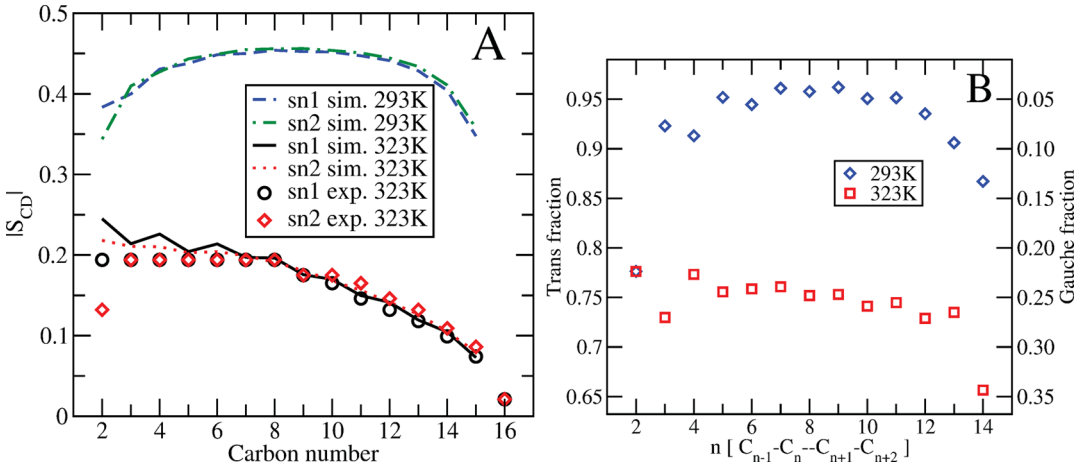

Figure 12. Alkane chain properties of the two phases in DPPC. *A:* Average order parameters of the alkane chains in the DPPC molecules. The experimental NMR data was retrieved from ref 55. *B:* The fraction of trans/gauche states as a function of the dihedral bond number.

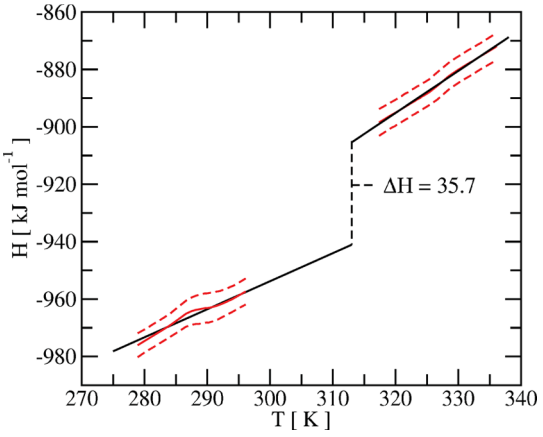

Figure 13. Total enthalpy per phospholipid without bulk water contribution. Red lines correspond to simulation data, while black lines are linear fits.

in Figure 13. We obtain an enthalpy at the melting temperature of 36 ± 5 kJ mol^{-1} and heat capacities C_p^f = 1460 ± 10 J mol^{-1} K^{-1} and C_p^g = 980 ± 10 J mol^{-1} K^{-1} for the fluid and gel phase, respectively. It should be noted that these do not take quantum mechanical excitations of the vibrational modes into account. The calculated phase transition enthalpy is quite close to the experimental value,[56] 36.5 kJ mol^{-1}. The calculated enthalpy change can be split into dihedral (30%), Lennard-Jones (60%), and electrostatic energy (10%). The dihedral energy change is consistent with a 20% change in the fraction of gauche bonds.

CONCLUSION

We have here shown that a slightly reparameterized UA force field for DPPC is needed to describe both the fluid and gel phases of membranes properly. We derive a relation for scaling *n*-alkane force field parameters without changing the densities of the higher alkanes, while increasing the potential energy and melting temperature of united atom hydrocarbons. The derived charges of the diacyl-PC headgroup yield dipole components in the range suggested by experiments. The modified force field produces a gel with correct area per lipid, tilt, and NMR order parameters. Structure factors calculated from atomic densities are in fair agreement with experimental X-ray and neutron scattering data. We also find the heat of melting in agreement with experiment. The simulations also shed some light on several issues that experiments have only partially or not at all resolved. This includes the observation that gel phase lipids have a small but non-negligible fraction of gauche bonds in the fatty acid chains as indicated by interpretations of Rahman scattering data. The orientation of the P−N-dipoles were not unexpectedly found to be uncorrelated with the orientation of the triangular lattice formed by the chains as well as the chain tilt direction. On the other hand, we found that the collective tilt direction is between two lattice vectors.

ASSOCIATED CONTENT

Supporting Information

A coordinate file and the other files necessary to run a gel simulation using GROMACS. This material is available free of charge via the Internet at http://pubs.acs.org.

AUTHOR INFORMATION

Corresponding Author

*E-mail: oed@kth.se.

Notes

The authors declare no competing financial interest.

ACKNOWLEDGMENTS

We thank professor John Nagle for valuable suggestions and discussions. This work has been supported by computer time allocation from SNIC (Swedish National Infrastructure for Computing) at the Parallel Computing Center at KTH (PDC) and has been partially funded by the Swedish Science Research Council (VR).

REFERENCES

(1) Egberts, E.; Berendsen, H. J. C. *J. Chem. Phys.* **1988**, *89*, 3718−3733.
(2) Tu, K.; Tobias, D.; Blasie, J.; Klein, M. *Biophys. J.* **1996**, *70*, 595−608.
(3) Venable, R. M.; Brooks, B. R.; Pastor, R. W. *J. Chem. Phys.* **2000**, *112*, 4822−4832.
(4) Goetz, R.; Lipowsky, R. *J. Chem. Phys.* **1998**, *108*, 7397−7409.
(5) Marrink, S. J.; Risselada, J.; Mark, A. E. *Chem. Phys. Lipids* **2005**, *135*, 223−244.
(6) Cooke, I. R.; Deserno, M. *Biophys. J.* **2006**, *91*, 487−495.
(7) Högberg, C.-J.; Nikitin, A. M.; Lyubartsev, A. P. *J. Comput. Chem.* **2008**, *29*, 2359−2369.

(8) Klauda, J. B.; Venable, R. M.; Freites, J. A.; O'Connor, J. W.; Tobias, D. J.; Mondragon-Ramirez, C.; Vorobyov, I.; MacKerell, A. D.; Pastor, R. W. *J. Phys. Chem. B* **2010**, *114*, 7830−7843.
(9) Jämbeck, J. P. M.; Lyubartsev, A. P. *J. Phys. Chem. B* **2012**, *116*, 3164−3179.
(10) Berger, O.; Edholm, O.; Jähnig, F. *Biophys. J.* **1997**, *72*, 2002−2013.
(11) Chiu, S.; Clark, M.; Balaji, V.; Subramaniam, S.; Scott, H.; Jakobsson, E. *Biophys. J.* **1995**, *69*, 1230−1245.
(12) Chiu, S.-W.; Pandit, S. A.; Scott, H. L.; Jakobsson, E. *J. Phys. Chem. B* **2009**, *113*, 2748−2763.
(13) de Vries, A. H.; Yefimov, S.; Mark, A. E.; Marrink, S. J. *Proc. Natl. Acad. Sci. U.S.A.* **2005**, *102*, 5392−5396.
(14) Tristram-Nagle, S.; Zhang, R.; Suter, R.; Worthington, C.; Sun, W.; Nagle, J. *Biophys. J.* **1993**, *64*, 1097−1109.
(15) Sun, W. J.; Sutter, R. M.; Knewtson, M. A.; Worthington, C. R.; Tristram-Nagle, S.; Zhang, R.; Nagle, J. F. *Phys. Rev. E* **1994**, *49*, 4665−4676.
(16) Marrink, S. J.; Risselada, H. J.; Yefimov, S.; Tieleman, D. P.; de Vries, A. H. *J. Phys. Chem. B* **2007**, *111*, 7812−7824 PMID: 17569554.
(17) Dickson, C. J.; Madej, B. D.; Skjevik, A.; Betz, R. M.; Teigen, K.; Gould, I. R.; Walker, R. C. *J. Chem. Theory Comput.* **2014**, *10*, 865−879.
(18) van der Spoel, D.; Lindahl, E.; Hess, B.; Groenhof, G.; Mark, A. E.; Berendsen, H. J. *J. Comput. Chem.* **2005**, *26*, 1701−1718.
(19) Darden, T.; York, D.; Pedersen, L. *J. Chem. Phys.* **1993**, *98*, 10089−10092.
(20) Bussi, G.; Donadio, D.; Parrinello, M. *J. Chem. Phys.* **2007**, *126*, 014101.
(21) Berendsen, H. J. C.; Postma, J. P. M.; van Gunsteren, W. F.; DiNola, A.; Haak, J. R. *J. Chem. Phys.* **1984**, *81*, 3684−3690.
(22) Parrinello, M.; Rahman, A. *J. Appl. Phys.* **1981**, *52*, 7182−7190.
(23) Car, R.; Parrinello, M. *Phys. Rev. Lett.* **1985**, *55*, 2471−2474.
(24) Abascal, J.; Vega, C. *J. Chem. Phys.* **2005**, *123*, 234505.
(25) Vega, C.; de Miguel, E. *J. Chem. Phys.* **2007**, *126*, 154707.
(26) Wohlert, J.; Edholm, O. *Biophys. J.* **1975**, *87*, 2433−2445, 2004.
(27) Braun, A. R.; Brandt, E. G.; Edholm, O.; Nagle, J. F.; Sachs, J. N. *Biophys. J.* **2011**, *100*, 2112−2120.
(28) Tsuzuki, S.; Honda, K.; Uchimaru, T.; Mikami, M. *J. Phys. Chem. A* **2004**, *108*, 10311−10316.
(29) Toxvaerd, S. *J. Chem. Phys.* **1990**, *93*, 4290−4295.
(30) Toxvaerd, S. *J. Chem. Phys.* **1997**, *107*, 5197−5204.
(31) Martin, M. G.; Siepmann, J. I. *J. Phys. Chem. B* **1998**, *102*, 2569−2577.
(32) Herrebout, W. A.; van der Veken, B. J.; Wang, A.; Durig, J. R. *J. Phys. Chem.* **1995**, *99*, 578−585.
(33) Ryckaert, J.-P.; Bellemans, A. *Chem. Phys. Lett.* **1975**, *30*, 123−125.
(34) Poger, D.; Van Gunsteren, W. F.; Mark, A. E. *J. Comput. Chem.* **2010**, *31*, 1117−1125.
(35) Jiemchooroj, A.; Sernelius, B. E.; Norman, P. *Phys. Rev. A* **2004**, *69*, 044701.
(36) CRC Handbook, *CRC Handbook of Chemistry and Physics, 88th Edition*, 88th ed.; CRC Press: 2007.
(37) Mashaghi, A.; Partovi-Azar, P.; Jadidi, T.; Nafari, N.; Maass, P.; Tabar, M. R. R.; Bonn, M.; Bakker, H. J. *J. Chem. Phys.* **2012**, *136*, 114709.
(38) Bechinger, B.; Seelig, J. *Biochemistry* **1991**, *30*, 3923−3929.
(39) Gawrisch, K.; Ruston, D.; Zimmerberg, J.; Parsegian, V.; Rand, R.; Fuller, N. *Biophys. J.* **1992**, *61*, 1213−1223.
(40) Kucerka, N.; Nagle, J. F.; Sachs, J. N.; Feller, S. E.; Pencer, J.; Jackson, A.; Katsaras, J. *Biophys. J.* **2008**, *95*, 2356−2367.
(41) Nagle, J. F.; Tristram-Nagle, S. *Biochim. Biophys. Acta* **2000**, *1469*, 159−161.
(42) Tristram-Nagle, S.; Liu, Y.; Legleiter, J.; Nagle, J. F. *Biophys. J.* **2002**, *83*, 3324−3335.
(43) Kucerka, N.; Nagle, J. F.; Katsaras, J. *J. Membr. Biol.* **2010**, *235*, 43−50.
(44) Kucerka, N.; Nieh, M.-P.; Katsaras, J. *Biochim. Biophys. Acta* **2011**, *1808*, 2761−2771.
(45) Kucerka, N.; Liu, Y.; Chu, N.; Petrache, H. I.; Tristram-Nagle, S.; Nagle, J. F. *Biophys. J.* **2005**, *88*, 2626−2637.
(46) Smith, G. S.; Sirota, E. B.; Safinya, C. R.; Plano, R. J.; Clark, N. A. *J. Chem. Phys.* **1990**, *92*, 4519−4529.
(47) Braun, A. R.; Sachs, J. N.; Nagle, J. F. *J. Phys. Chem. B* **2013**, *117*, 5065−5072.
(48) Kucerka, N.; Perlmutter, J. D.; Pan, J.; Tristram-Nagle, S.; Katsaras, J.; Sachs, J. N. *Biophys. J.* **2008**, *95*, 2792−2805.
(49) Leekumjorn, S.; Sum, A. K. *Biochim. Biophys. Acta* **2007**, *1768*, 354−365.
(50) Schubert, T.; Schneck, E.; Tanaka, M. *J. Chem. Phys.* **2011**, *135*, 1−11.
(51) Brandt, E. G.; Edholm, O. *J. Chem. Phys.* **2010**, *133*, 115101.
(52) Nagle, J. F. *Biophys. J.* **1993**, *64*, 1110−1112.
(53) Davis, J. H. *Biophys. J.* **1979**, *27*, 339−358.
(54) Yellin, N.; Levin, I. W. *Biochemistry* **1977**, *16*, 642−647.
(55) Leftin, A.; Brown, M. F. *Biochim. Biophys. Acta* **2011**, *1808*, 818−839.
(56) Albon, N.; Sturtevant, J. M. *Proc. Natl. Acad. Sci. U.S.A.* **1978**, *75*, 2258−2260.